# Chapter 3

## A Low Cost Carbon Black/Polyaniline Nanotube Nanocomposite as Efficient Electro-catalyst for Triiodide Reduction in Dye Sensitized Solar Cells

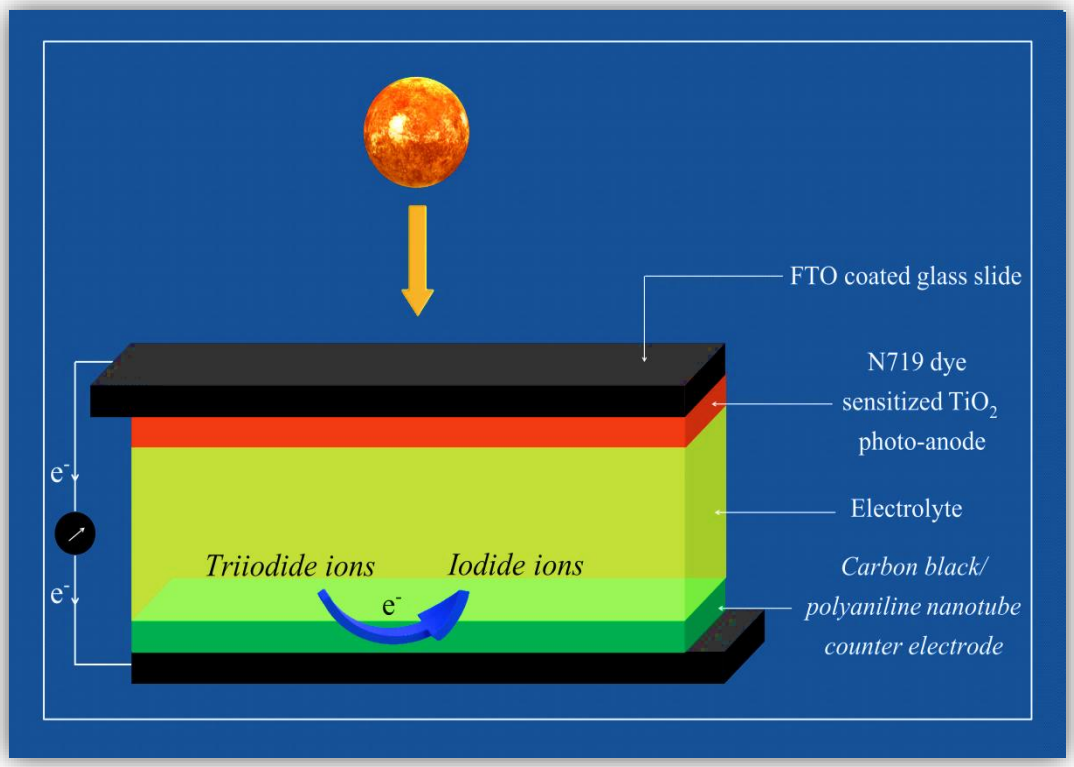


A carbon black/polyaniline nanotube nanocomposite is synthesized *via in situ* oxidation polymerization reaction for application as a low-cost platinum-free counter electrode in dye sensitized solar cell for reduction of triiodide ions.

## 3.1 Introduction

Solar energy is becoming a focus of worldwide attention as the panacea for the current energy crisis surrounding depleting oil reserves and environmental pollution. In the last couple of decades, dye sensitized solar cells (DSSCs) have emerged as a clean energy system that harvest sunlight and convert it directly into electrical energy. Successfully demonstrated by B. O'Regan and M. Gratzel for the first time in 1991, DSSCs make very popular candidates as credible alternatives for conventional solar cells because of their cost effectiveness, simple fabrication technique and relatively high energy conversion efficiency [1]. In fact, conversion efficiency of upto 13% has been realized recently [2,3]. DSSCs differ from silicon based solar cells in the aspect that their light absorption and charge carrier transport components are separate. A dye sensitized photoanode as working electrode, a counter electrode (CE) and an electrolyte containing triiodide/iodide ($I_3^-/I^-$) redox couple generally constitute the three main components of a DSSC [4,5]. CE performs the dual function of transferring electrons to the electrolyte from the external circuit as well as acting as a catalyst to reduce the $I_3^-$ ions. Platinum (Pt) serves as an ideal candidate for CE because of its low charge transfer resistance and high exchange current densities. However, limited reserve and expensiveness of Pt limit its application for large scale production. Additionally, it can be corroded by the electrolyte to give platinum iodide, ($PtI_4$) [6]. Therefore, it is desirable to develop low cost CEs that exhibit superior catalytic behavior and strong corrosion resistance.

Intrinsically conducting polyaniline (PAni) is one of the most intensively studied polymers due to its high conductivity, good environmental stability, inexpensiveness and excellent catalytic activity for $I_3^-$ reduction. Li *et al.* published the first report on construction of PAni nanoparticles based CE for which they obtained an efficiency of 7.15% [7]. Since then other groups have also been employing PAni as CEs and efficiency of upto 11.6% has already been achieved [8]. PAni nanotubes (PAniNTs), a class of one-dimensional nanostructures (ODNS), owing to their dimensionality, possess long conjugation length and high degree of

---

*This part of the thesis is published in:*

Bora, A., Mohan, K., Phukan, P., and Dolui, S. K. A low cost carbon black/polyaniline nanotube composite as efficient electro-catalyst for triiodide reduction in dye sensitized solar cells. *ElectrochimicaActa,* 259:233-244, 2018.

electron delocalization. Both these factors contribute to exhibit superior electrical conduction and electrocatalytic behavior towards the redox couple [9,10]. But there is a probability of PAni dispersing into the electrolyte, resulting in peeling off of the films and thus negatively affecting the efficiency of the DSSC [11].

Carbon based materials, on the other hand, have excellent corrosion resistance [12]. There have been many reports on application of these materials as CEs [13,14]. Carbon black (CB), in particular, has many advantages due to its mesoporous structure, which generates a large active surface area. The electrolyte can be trapped within the pores increasing the interface between the electrolyte and the CE [15]. Moreover, CB has low crystallinity and more edges in comparison to highly oriented carbon materials like graphite and carbon nanotubes. Since the active sites for reduction of $I_3^-$ are located at the edges, CB is more active towards catalysis of the redox couple [16]. But the conversion efficiency of carbon materials obtained so far is low in comparison to PAni nanoparticles. Furthermore, both PAni and CB suffer from shortage of self-adhesion [11]. But there have been reports of a site-selective interaction between PAni and carbon, that can enhance the adhesion of PAni film on the substrate [17]. Nanocomposites comprising of PAni and CB are expected to incorporate the pros of both the constituents and hence, provide an optimistic outlook for replacement as CEs. Looking at the literature, there are several published works on the use of nanocomposites of carbon based materials and PAni as CEs [11,18]. For instance, Wang *et al.* prepared PAni/graphene hybrid CEs where the conversion efficiency reached 6.09% under illumination of light (100 mW $cm^{-2}$) [19]. However, very few articles focus particularly on CB/PAni nanocomposite. Ikeda *et al.* prepared clay-like CE material based on polyaniline loaded CB and an ethyleneoxide-substituted imidazolium iodide. The material showed a maximum efficiency of 4.07% for 23 mW $cm^{-2}$ irradiation[20].

In this work, we report the template free synthesis of PAniNT and CB/PAniNT nanocomposite with different weight percentages (wt%) of CB *viain situ* chemical oxidation polymerization technique. The CB/PAniNT nanocomposites are investigated as potential CE material for DSSCs. Cyclic voltammetry (CV) studies indicate their promising property as an electro-catalyst having catalytic activity at par with Pt as CE. The ratio of $[I_2]/[I^-]$ in the electrolyte is varied to obtain the optimum results. Furthermore, the effect of film thickness on the photovoltaic performance of the DSSCs is also measured by electrochemical impedance spectroscopy (EIS) and photocurrent density *vs.* voltage (*J-V*) characteristics in both liquid electrolyte (LE) as well as polymer gel electrolyte (PGE).

## 3.2 Materials and methods

### 3.2.1 Chemicals

All the chemicals including aniline, ammonium peroxydisulphate (APS), acetonitrile, titanium tetrachloride ($TiCl_4$), mesoporous CB, di-tetrabutylammonium *cis*-bis(isothiocyanato)bis(2,2'-bipyridyl-4,4'-dicarboxylato)ruthenium(II) (N719), titanium dioxide ($TiO_2$), chloroplatinic acid ($H_2PtCl_6$), sodium borohydride ($NaBH_4$), lithium perchlorate ($LiClO_4$), lithium iodide (LiI), iodine ($I_2$) tertbutylpyridine (TBP), 1-methyl-3-propylimidazolium iodide (MPI) and N-methyl-2-pyrrolidone (NMP) purchased from Sigma-Aldrich were analytical reagent grade chemicals and used as received. Fluorine doped tin oxide (FTO) glass substrate was also procured from Sigma.

### 3.2.2 Synthesis of CB/PAniNT nanocomposite

PAniNTs were prepared by chemical oxidation polymerization of aniline described in *Section 2.2.2.1 of Chapter 2*. For synthesis of CB/PAniNT nanocomposites with different contents of CB: 0.5, 0.75 and 1.0 wt%, *in-situ* polymerization of aniline in the presence of CB was followed. The CB nanoparticles, dispersed in distilled water by sonicating them for 2 hours, were directly added to the reaction mixture containing the aniline monomer. The other reaction parameters were kept same. The resulting precipitate obtained after the completion of the reaction contained the required nanocomposites.

### 3.2.3 Fabrication of DSSCs

For fabrication of $TiO_2$ photoanode, the FTO coated glass substrates were initially treated with 40 mM $TiCl_4$ solution at 70 ºC for 30 min. It was followed by their sintering at 400 ºC for 30 min to ensure proper contact between the glass and $TiO_2$. After cooling to room temperature, $TiO_2$ paste prepared in ethanol was applied on the pre-treated area using spin coating technique. The films were dried at room temperature and again sintered at 450 ºC for 30 min. After cooling to room temperature, the $TiO_2$ coated electrodes were immersed in 0.3 mM N719 dye prepared in acetonitrile/ethanol (1:1 volume ratio) solvent for 24 h. Following that, the dried N719 sensitized $TiO_2$ electrodes were used as photo-anodes in DSSCs.

To fabricate CB/PAniNT CE, a smooth paste of the nanocomposite was prepared by adding the powder in 0.1% Nafion solution. The paste was deposited onto FTO coated glass substrate by doctor blade method. After that, the electrodes were heated at 80 ºC for 60 min. The CB/PAniNT coated glass electrodes were used as CEs. To prepare Pt CE, the cleaned FTO

coated glass slide was coated with $H_2PtCl_6$ to deposit a layer of Pt, followed by reduction with $NaBH_4$.

LE used in DSSCs comprised of LiI, $I_2$, 0.5 M TBP and 0.6 M MPI in a mixed solvent of NMP and acetonitrile (volume ratio 1:4). The amount of LiI and $I_2$ were fixed at 0.5 M and 0.05 M respectively. NMP was added to acetonitrile in the mixed solvent to improve the long-term stability of DSSCs due to low volatility of NMP [21]. The poly(methyl methacrylate) (PMMA)/PAniNT PGE was prepared according to the procedure previously developed by our group [22]. The electrolytes were dropped on the CE and then the dye sensitized $TiO_2$ photoanode was clipped over it tightly using two clips to fabricate two different types of sandwich-type DSSCs, one with LE and the other with PGE. 25 µm thick Solaronix thermal polymer spacers were used between the two electrodes to avoid contact between them.

### 3.2.4 Characterization

The instruments used to record the Fourier transform infra-red (FTIR) spectra and transmission electron microscope (TEM) micrographs of the samples are described in *Section 2.2.3.1 of Chapter 2*. Additionally, a Renishaw basis series with 514 lasers was used to obtain the Raman spectra.Scanning electron microscope (SEM) micrographs at an acceleration voltage of 20 kV were obtained by a JEOL JSM-6390 LV SEM instrument. The film thickness was measured by a SurtronicS-100 series profilometer. Bio-Logic SP-150 potentiostat was used to perform CV measurements with silver/silver chloride (Ag/AgCl) as reference electrode, a Pt wire as CE and thin films of the nanocomposite powders deposited on FTO coated glass slide as working electrode. A standard solution of 0.01 M LiI, 0.001 M $I_2$ and 0.1 M $LiClO_4$ in acetonitrile was used as supporting electrolyte and the scan rate was kept at 50 mV $s^{-1}$. The same instrument was also used to carry out EIS measurements. The *J-V* characteristics were recorded under 1 sun illumination (generated by a solar simulator with xenon arc lamp with irradiation of 100 mW $cm^{-2}$). The fill factor (*FF*) and photo-conversion efficiency ($\eta$) were calculated from the *J-V* characteristics by applying **relations (3.1)** and **(3.2)**.

$$FF = \frac{(J_{max} \times V_{max})}{(J_{SC} \times V_{OC})} \quad \textbf{(3.1)}$$

$$\eta = \frac{(J_{max} \times V_{max})}{P_{in}} \times 100 \quad \textbf{(3.2)}$$

where$J_{max}$ (mA $cm^{-2}$), $V_{max}$ (V), $J_{SC}$(mA $cm^{-2}$), $V_{OC}$ (V) and $P_{in}$ (100 mW $cm^{-2}$) are the maximum current density, maximum voltage, short-circuit current density, open-circuit voltage and incident light power respectively.

## 3.3 Results and discussion

**3.3.1 FTIR spectra analyses.Figure 3.1** shows the FTIR spectra of CB and 0.75 wt% CB/PAniNT nanocomposite. The FTIR spectrum of PAniNT is shown in *Section 2.3.1* of *Chapter 2*. In the FTIR spectrum of CB, a peak appears at 3439 $cm^{-1}$ corresponding to -OH stretching [23]. The bands at 2916 $cm^{-1}$ and 2852 $cm^{-1}$ come from symmetric and asymmetric CH vibrations in $CH_2$ and $CH_3$ groups [24]. The bands at 1571 $cm^{-1}$ and 570 $cm^{-1}$ are attributed to conjugated C=O in quinine moiety and aromatic hydrogen stretching respectively. The results indicate that functional groups like hydroxyl, carbonyl and carboxyl groups that contain oxygen cover the surface of CB [23], which contributes to its ability to form composites with PAniNT. The FTIR spectrum of CB/PAniNT appears similar to that of pristine PAniNT. The absorbance peaks of CB are greatly concealed by PAniNT.

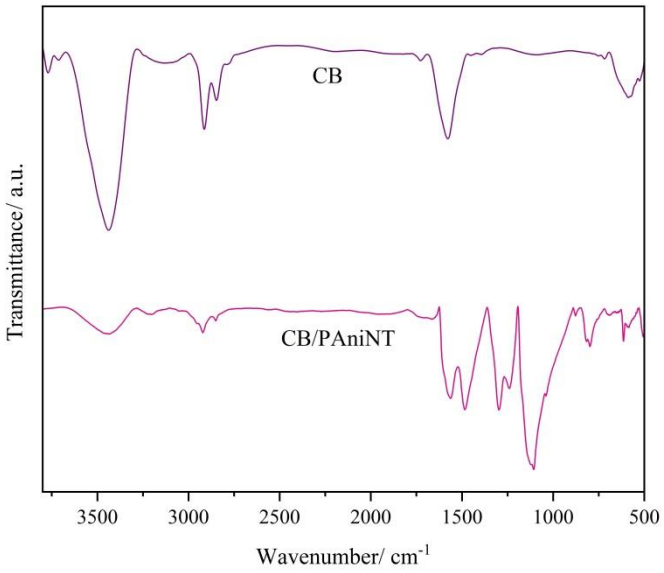


**Figure 3.1** FTIR spectra of CB and 0.75 wt% CB/PAniNT nanocomposite.

**3.3.2 Raman spectra analyses.Figure 3.2** shows the Raman spectra of PAniNT, CB and CB/PAniNT (0.75 wt%) nanocomposite. In the PAniNT spectrum, C-H band in plane bending vibration of quinoid ring appears around 1200 $cm^{-1}$. The semi-benzoid polaronic ν(C-N+•) band, the imine ν(C=N) vibration band and the ν(C=C) band appear at 1350, 1550 and 1620 $cm^{-1}$ respectively [25]. CB, on the other hand, have a couple of Raman-active bands, with the D band appearing at 1375 $cm^{-1}$ and G band at 1616 $cm^{-1}$ corresponding to defects or edge areas and vibration of $sp^2$-hybridized carbon respectively [26]. The individual identities of each component are retained in the CB/PAniNT nanocomposite. However, the bands of CB are camouflaged by PAniNT since they appear in the same range.

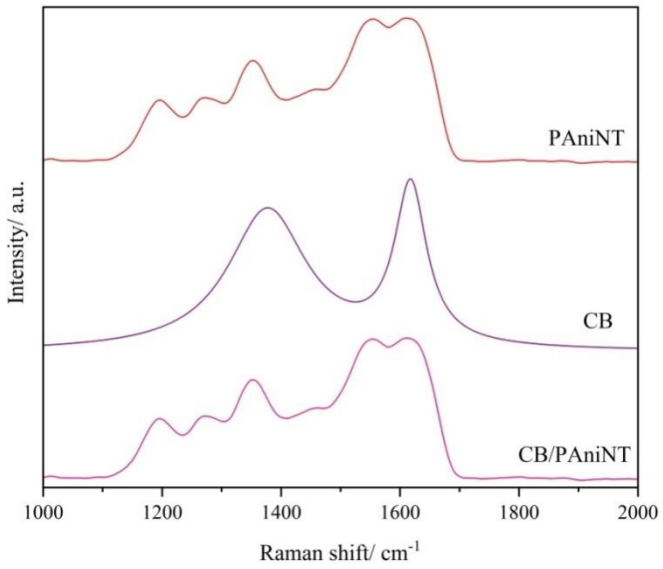


**Figure 3.2** Raman spectra of PAniNT, CB and 0.75 wt% CB/PAniNT nanocomposite.

**3.3.3 Morphological analyses.**Surface morphology of the 0.75 wt% CB/PAniNT nanocomposite and the individual components are investigated by SEM and TEM. CB appears as small grains as seen in its SEM micrograph **(Figure 3.3 (a))**. In the SEM **(Figure 3.3 (b))** and TEM **(Figure 3.3 (c))** images of 0.75 wt% CB/PAniNT, the tubular nature of PAniNT remains intact. However, there is an increase in the diameter of PAniNT **(*Figure 2.5 (a)* of *Chapter 2*** shows the TEM image of PAniNT**)**. This result leads to the conclusion that CB nanoparticles are

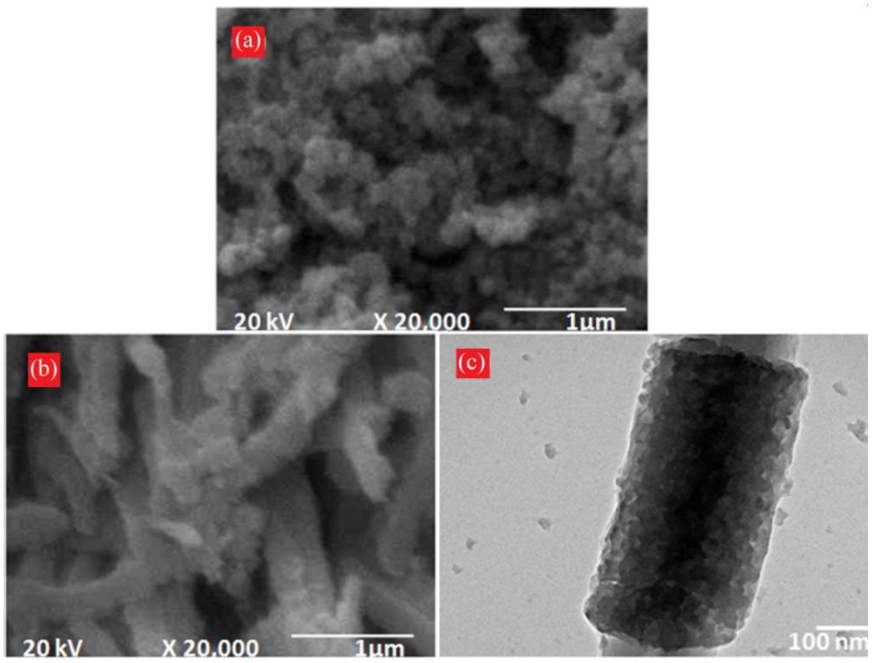


**Figure 3.3** SEM micrographs of **(a)** CB and **(b)** 0.75 wt% CB/PAniNT nanocomposite, and **(c)** TEM micrograph of 0.75 wt% CB/PAniNT nanocomposite.

deposited on the surface of the PAniNT. The presence of the mesoporous CB layer can be held accountable for an increase in the surface area of the composite.

**3.3.4 Conductivity of the composites.**High electrical conductivity for transportation of electrons along with high electro-catalytic activity for reduction of the electrolyte are the pre-requisites for the selection of a material as CE in DSSCs [27]. Conduction in PAni takes place *via* polaron and bipolaron defects [28]. Although the conduction mechanism in three-dimensional structures has been extensively studied, a generalized trend has not yet been established for ODNS. Nonetheless, work with polypyrrole (PPy) nanotubes has led to the observation that the nanotubes contain a significant number of bipolarons in contrast to PPy films, where bipolaron concentration is nil. The authors credited the higher conductivity of PPy nanotubes to higher concentration of bipolaron and a longer conjugation length [29]. Similarly, Li *et al.* observed higher conductivity for PPy nanotubes in comparison to globular ones [30]. The reason for this observation was proposed to be better connections and crossing of the nanotubes with high aspect ratio for forming a conducting network. If these properties are applied to PAniNT, then an enhanced conductivity can be expected. R. V. Parthasarathy and C. R. Martin have shown that the conductivity of hard-template synthesized PAniNTs with smaller diameter show higher conductivity than conventional PAni powder, and reaches comparable values only when the diameter is as high as 400 nm [31].

The conductivity value of PAniNT obtained by four probe method is 0.028 S $cm^{-1}$. The synthesis procedure applied in this work employs weakly acidic acetic acid to produce nanotubular structures having hydrogen sulfate as counter ions. During oxidation of aniline by APS in the presence of acetic acid, the PAniNT produced is protonated by sulfuric acid formed as a by-product during the reaction **(Scheme 3.1)**[32]. The amount of sulfuric acid produced

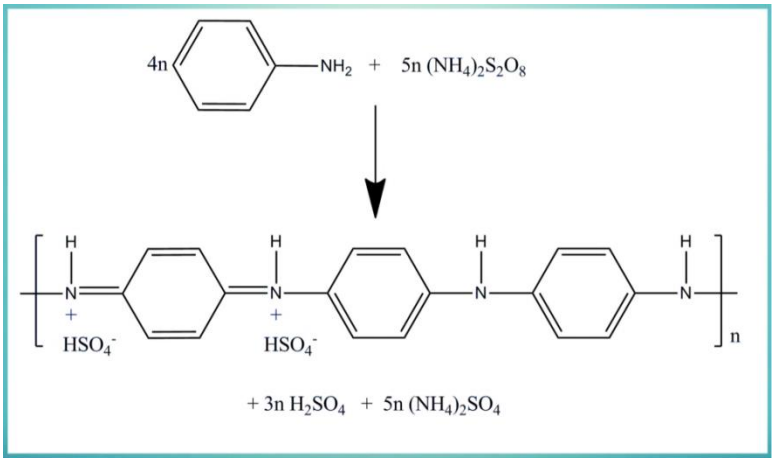


**Scheme 3.1** Reaction scheme of aniline with APS to give the hydrogen sulfate salt and producing sulfuric acid as by-product.

during the reaction is capable of fully protonating the PAniNT. On introducing CB, it is seen that there is an increase in the electrical conductivity of the PAniNT upto 0.75 wt% loading **(Table 3.1)**. This result is mainly attributed to the fact that CB, with a large effective surface area can act as a "conducting bridges" to join the different conducting PAni domains [33].

**Table 3.1** Conductivity measurements of the prepared samples.

| Compound | Amount of CB/ wt% | Conductivity/ S $cm^{-1}$ |
|---|---|---|
| PAniNT | 0 | 0.028 |
| CB/PAniNT | 0.5 | 3.562 |
| CB/PAniNT | 0.75 | 4.057 |
| CB/PAniNT | 1.0 | 3.195 |

**3.3.5 Catalytic activity of the composites.**CV was employed to investigate the catalytic property of the CB/PAniNT nanocomposites towards $I_3^-$ reduction, and compare it with that of Pt. Peak current ($E_P$) and peak to peak separation ($E_{PP}$) are two important parameters that are used to determine the catalytic performance of CEs. Higher $E_P$ and lower $E_{PP}$ values indicate better electro-catalytic behavior. **Figure 3.4** shows the cyclic voltammograms of pristine PAniNT, CB, CB/PAniNT nanocomposites and Pt. Each material exhibits two anodic and two cathodic current peaks analogous to **relations (3.3)** and **(3.4)**.

$$3I^- \leftrightarrow I_3^- + 2e^- \quad \textbf{(3.3)}$$

$$2I_3^- \leftrightarrow 3I_2 + 2e^- \quad \textbf{(3.4)}$$

The positions of the peaks are, however, slightly different in each case. The 0.75 wt% CB/PAniNT nanocomposite shows maximum resemblance to Pt electrode in terms of catalytic activity. The current density of the left redox pair of 0.75 wt% CB/PAniNT (anodic peak current density is 9.257 mA $cm^{-2}$ and cathodic peak current density is -5.242 mA $cm^{-2}$), responsible for reduction of $I_3^-$ to $I^-$ in DSSCs [34,35], is slightly higher than Pt (anodic peak current density is 8.867 mA $cm^{-2}$ and cathodic peak current density is -5.086 mA $cm^{-2}$). Higher current densities can be attributed to the larger active surface area of mesoporous CB, enabling faster redox reaction at the CE [36]. In addition, the left redox $E_{PP}$ value, calculated by using **relation (3.5)** can also be inversely correlated with the rate of $I_3^-$ to $I^-$ reduction.

$$E_{PP} = E_P(anodic) - E_P(cathodic) \quad \textbf{(3.5)}$$

The $E_{PP}$ value of Pt is 0.84 V while that of 0.75 wt% CB/PAniNT nanocomposite is 0.82 V. This result further emphasizes that 0.75 wt% nanocomposite shows superior catalytic activity and can be used as a potential CE in DSSCs.

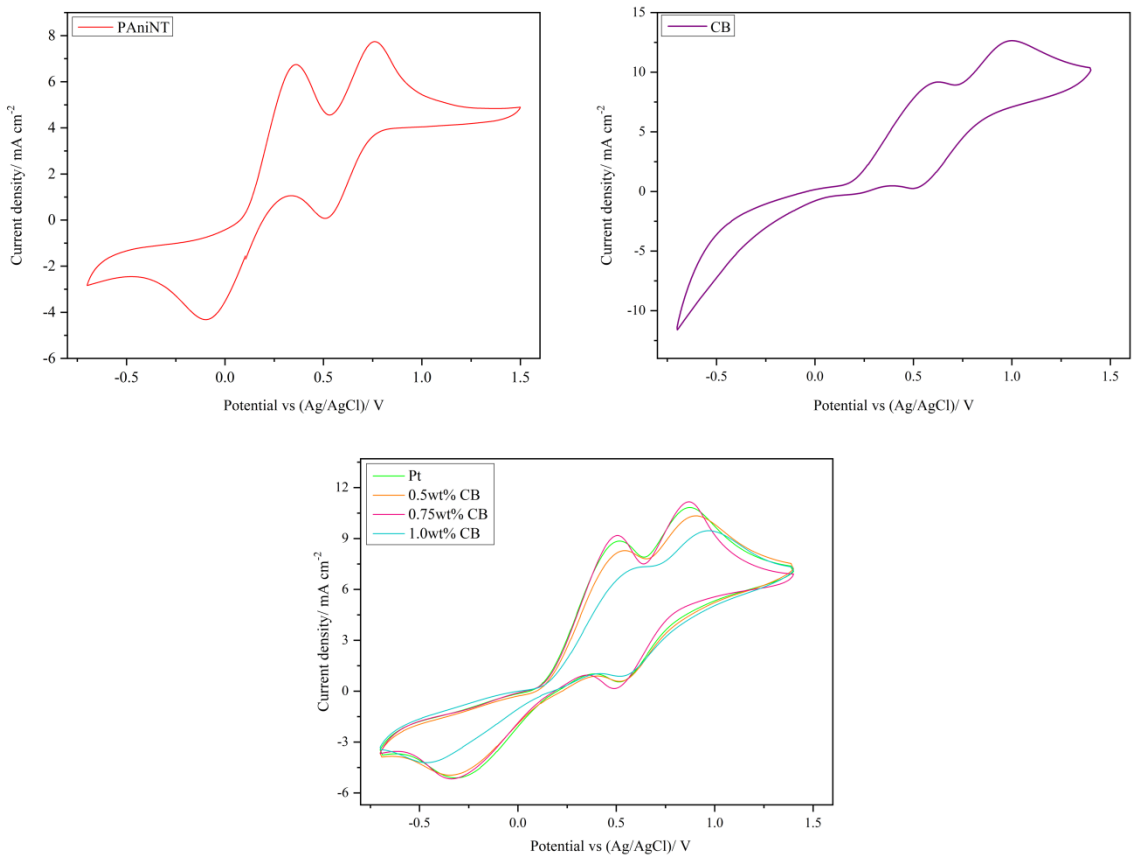


**Figure 3.4** Cyclic voltammograms of PAniNT, CB, Pt and CB/PAniNT nanocomposites with 0.5, 0.75 and 1.0 wt% CB.

### 3.3.6 Photovoltaic performance of the DSSCs.

***3.3.6.1 Effect of variation of [$I_2$]/[$I^-$] ratio:*** To better understand the redox conditions, photovoltaic parameters, $V_{OC}$ and $J_{SC}$, of pristine PAniNT CE based DSSCs were studied for different [$I_2$]/[$I^-$] ratios. The involvement of the redox couple in the working of a DSSC can be seen in the **relations (3.6 (a)-(e))**:

$$3I^- (electrolyte) \rightarrow I_3^- (electrolyte) + 2e^- (TiO_{2 conduction\ band}) \text{ (at photoanode)} \quad \textbf{(3.6 (a))}$$

$$I_3^- (electrolyte) + 2e^- (CE) \rightarrow 3I^- (electrolyte) \text{ (at CE)} \quad \textbf{(3.6 (b))}$$

$$I_3^- (electrolyte) + 2e^- (TiO_{2 conduction\ band}) \rightarrow 3I^- (electrolyte) \text{ (recombination)} \quad \textbf{(3.6 (c))}$$

$3I^-(electrolyte) + 2\ dye^+ \rightarrow 2\ dye + I_3^-$ (regeneration of dye) **(3.6 (d))**

$dye^+ + e^-(TiO_{2conduction\ band}) \rightarrow dye$ (recombination) **(3.6 (e))**

$V_{OC}$ is the difference between the Fermi level of the $TiO_2$ photoanode under illumination and the redox potential of the electrolyte ($E_{redox}$). $E_{redox}$ is given by **relation (3.7)**:

$$E_{redox} = E_o + {R'T}/{n'F}\ ln\ {[I_3^-]}/{[I^-]^3} \quad \textbf{(3.7)}$$

where$E_o$, *R'* and *T* represent standard potential, universal gas constant and absolute temperature respectively. *n'* is the number of electrons involved in the redox reaction (i.e. 2). It follows from the equation that by varying the concentration of the redox couple, $V_{OC}$ can be manipulated.

$$I_2 + I^- \leftrightarrow I_3^- \quad \textbf{(3.8)}$$

The equilibrium constant for the **relation (3.8)** is $10^{6.78}$[37]. Since this value is quite high, increasing the concentration of $I_2$ will produce a higher amount of $I_3^-$ in the electrolyte. Thus, the recombination process between the electrons of the conduction band of the $TiO_2$ and $I_3^-$ ions of the electrolyte **(relation 3.6 (c))** accelerates, as a consequence of which the value of $V_{OC}$ decreases [38]. This effect of $[I_3^-]$ on $V_{OC}$ is also very evident from **relation (3.9)**:

$$V_{OC} = {k'T}/{q'u\alpha}\ ln({I_{inj}}/{n_o^{u\alpha}k_{et}[I_3^-]}) \quad \textbf{(3.9)}$$

where *k', q', $I_{inj}$, $n_o$,* and$k_{et}$ are the Boltzmann constant, charge of the electron, charge flux from an electron injection by the oxidized dye, electron concentration at the $TiO_2$ surface in the dark and the rate constant for the reduction of $I_3^-$ by the conduction band electrons respectively.

Different concentrations of $I_2$ were used for preparing the electrolyte: 0.05, 0.1, 0.25 and 0.5 M, while the ratio of $[I_2]/[I^-]$ was varied as 1:2, 1:5 and 1:10. From **Figure 3.5 (a)**, it is seen that for all the three ratios of $[I_2]/[I^-]$, there is a decrease in the value of $V_{OC}$ when $[I_2]$ is increased. This result fits in completely with the effect of recombination kinetics described above. The decrease in $V_{OC}$ with increasing $[I^-]$ at fixed $[I_2]$, on the other hand, is a consequence of the irreversible intercalation of $Li^+$ ions (present in the electrolyte) with $TiO_2$ [39]. The electrons, present on the surface of $TiO_2$ because of the injection from the oxidized dye, easily attract the $Li^+$ ions. This is a non-Faradic process which results in the formation of an electrochemical double layer (EDL) at the interface between $TiO_2$ photoanode and the electrolyte. The potential drop in this layer causes a positive shift in the conduction band potential of $TiO_2$ and lowers $V_{OC}$[40]. The higher number of $Li^+$ ions, on the other hand, exerts a positive influence on the $J_{SC}$ values. It forms ambipolar $Li^+e^-$, which fastens the electron

transportation process through the photoanode and increases $J_{SC}$ at higher ratios of $[I_2]/[I^-]$ **(Figure 3.5 (b))**[41]. Additionally when $[I^-]$ is high, it aids in regeneration of the oxidized dye (**relation (3.6 (d))**, thereby inhibiting the regeneration of the dye by the injected electrons of $TiO_2$ photoanode **(relation (3.6 (e))**. Both these factors account for a high $J_{SC}$ value when $[I_2]/[I^-]$ ratio is 1:10. However, increasing $[I_2]$ facilitates the recombination process of **relation (3.6 (c))**. $I_2$ can also act as a dopant for conducting polymers like PAni, thereby increasing its conductivity [41]. So, two opposing effects are in action. In our case, the recombination reaction predominates as a result of which $J_{SC}$ decreases slightly with increasing $I_2$ concentration [42].

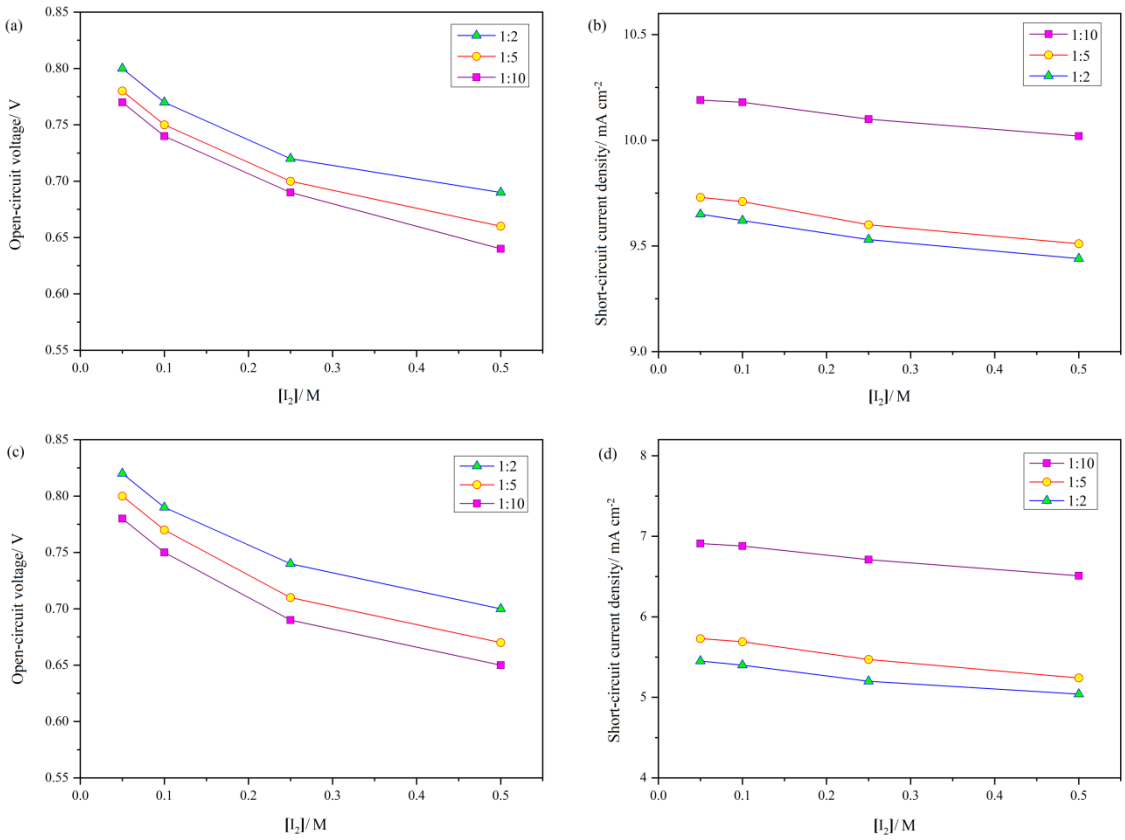


**Figure 3.5** Variation of $V_{OC}$ and $J_{SC}$ values of PAniNT with $[I_2]$ for $[I_2]/[I^-]$ ratios of 1:2, 1:5 and 1:10 in **(a, b)** LE and **(c, d)** PGE respectively.

The effects of variation of $[I_2]/[I^-]$ ratio seen with both LE and PGE are similar in trend. However, with PGE, the formation of EDL is hindered since $Li^+$ ions get attracted by electron rich oxygen of ester moieties. This leads to a higher $V_{OC}$ in PGE in comparison to LE **(Figure 3.5 (c))**. Also, due to higher viscosity of the polymer gel network, mobility of ions is restricted which is considered responsible for the lower values of $J_{SC}$ in PGE **(Figure 3.5 (d))**[43]. It is noteworthy that for variation of $[I_2]/[I^-]$ ratios, $V_{OC}$ and $J_{SC}$ are inversely related, so the challenge is to find a compromise between the two to get better performance. The efficiency of a DSSC is most correlated to $J_{SC}$[44]. Hence, from the results obtained, it can be concluded that the

optimum concentration of $I_2$ for electrolyte preparation is 0.05 Mhaving $[I_2]/[I^-]$ ratio of 1:10. And as such, these values are used for preparing our prototype DSSCs for further evaluation.

***3.3.6.2 Effect of variation of CB content:*** The photovoltaic performance characteristics of the CE are deduced from the maximum current obtained by the cells under short circuit conditions. In LE, under light intensity of 100 mW $cm^{-2}$,$J_{SC}$ 10.19 mA $cm^{-2}$ and $V_{OC}$ 0.77 V are exhibited by pristine PAniNT which leads to a moderate $\eta$ of 4.27% **(Table 3.2)**. But with the incorporation of CB, a gradual increase in $J_{SC}$ and decrease in $V_{OC}$is seen until percolation threshold is reached at 0.75 wt% CB **(Figure 3.6 (a))**. This composition corresponds to $J_{SC}$ 11.86 mA $cm^{-2}$, $V_{OC}$ 0.75 V and $\eta$ 5.96%. The enhancement in $J_{SC}$ values is a manifestation of comparatively high conductivity and electrocatalytic activity of the nanocomposite for $I_3^-$ to $I^-$ reduction which provides a faster passage for charge transport [19]. On the other hand, undesirable dark current of the device which is considered responsible for a negative shift in the energy band levels of the $I_3^-/I^-$ redox couple, can be accounted for causing a slight decrease in $V_{OC}$[11,45] In the photon to current conversion process, the voltage loss incurred together with local iodide concentration play a crucial part in the regeneration of the sensitizer [46]. The interplay of all these factors finally results in exceptional efficiency of the nanocomposite whose value is comparable to that of Pt (6.75%). However, further increase in CB content causes agglomeration and hinders charge transportation, which hampers the overall cell performance. The nanocomposites behave in a similar manner in PGE and an optimized device with 0.75wt% CB/PAniNT shows $\eta$ 4.39% with $J_{SC}$ 8.70 mA $cm^{-2}$ and $V_{OC}$ 0.75 V **(Figure 3.6 (b))**. Pt CE under analogous conditions exhibits 5.13% efficiency. The results obtained thus far allude to the feasibility of the nanocomposite to act as CE in DSSCs comprising both LE and PGE.

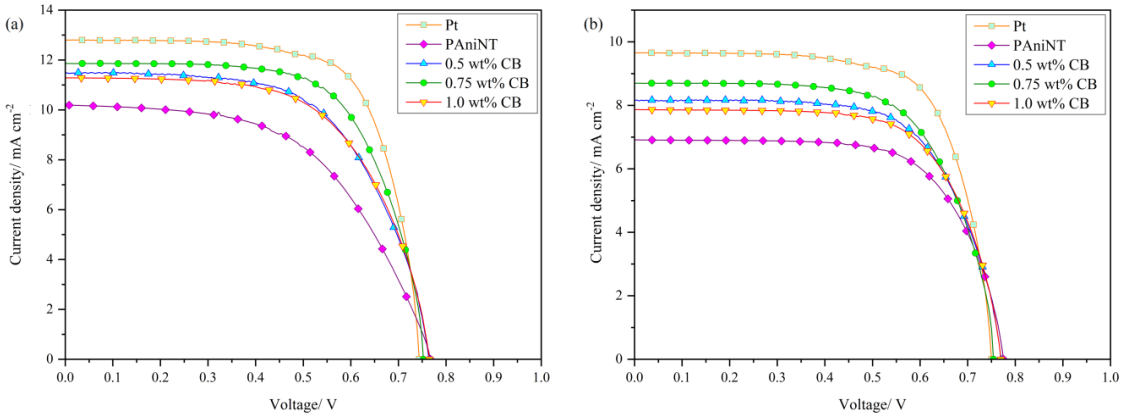


**Figure 3.6***J-V* characteristics of DSSCs fabricated with Pt, PAniNT and CB/PAniNT (with 0.5, 0.75 and 1.0 wt% CB) CE in **(a)** LE and **(b)** PGE.

**Table 3.2** Photovoltaic parameters of the DSSCs with Pt, PAniNT and CB/PAniNT CE in LE and PGE.

| Electrolyte | Counter electrode | $V_{OC}$/ V | $J_{SC}$/ mA cm$^{-2}$ | *FF* | $\eta$/ % |
|---|---|---|---|---|---|
| *Liquid electrolyte* | Pt | 0.74 | 12.79 | 0.71 | 6.75 |
| | PAniNT | 0.77 | 10.19 | 0.54 | 4.27 |
| | CB/PAniNT (0.5) | 0.76 | 11.46 | 0.61 | 5.36 |
| | CB/PAniNT (0.75) | 0.75 | 11.86 | 0.67 | 5.96 |
| | CB/PAniNT (1.0) | 0.76 | 11.28 | 0.61 | 5.30 |
| *Polymer gel electrolyte* | Pt | 0.75 | 9.65 | 0.71 | 5.13 |
| | PAniNT | 0.78 | 6.91 | 0.68 | 3.63 |
| | CB/PAniNT (0.5) | 0.77 | 8.16 | 0.67 | 4.19 |
| | CB/PAniNT (0.75) | 0.75 | 8.70 | 0.67 | 4.39 |
| | CB/PAniNT (1.0) | 0.77 | 7.87 | 0.68 | 4.10 |

***3.3.6.3 Effect of thickness variation:*** A critical point indicative of the maximum photo-conversion efficiency was reached at 0.75 wt% CB. Therefore, we used 0.75 wt% CB/PAniNT to study the effect of thickness variation on the photovoltaic performance of the DSSCs employing LE **(Figure 3.7 (a))** and PGE **(Figure 3.7 (b))**. The notations CBP_1, CBP_2, CBP_3 and CBP_4 represent thicknesses of 0.78 µm, 1.56 µm, 7.24 µm and 10.58 µm respectively. In the devices, growing thickness is found to cause an enhancement in its efficiency. Increase in

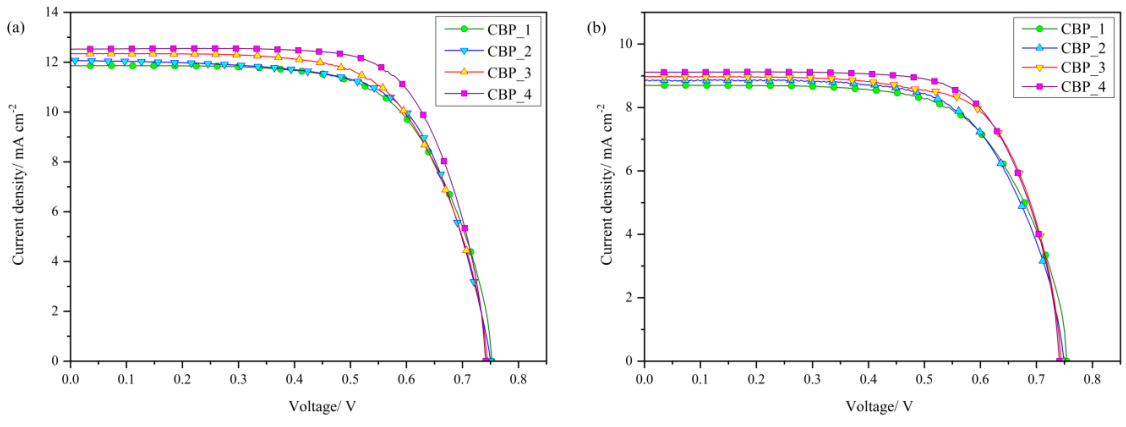


**Figure 3.7**Effect of thickness variation on the *J-V* characteristics of 0.75 wt% CB/PAniNT CE based DSSC in **(a)** LE and **(b)** PGE.

thickness of the CE from 0.78 μm to 10.58 μm causes 5.97% improvement in its FF in both LE and PGE **(Table 3.3)**. This improvement in the photovoltaic performance is even more pronounced when we consider the efficiency of the DSSCs. A 10.58 μm thick ideal device shows 6.62% η in LE. For a cell with the same thickness in PGE, η value is 4.82%. This can be considered as a manifestation of the heterogeneous electron transfer overvoltage losses in the thinner layers. When the layers are thin, there is insufficient catalytic activity but increase in thickness increases the reduction rate of $I_3^-$, which in turn reduces overvoltage losses [16]. Increasing thickness, thus, understandably exert a positive influence on the device behavior upto 10-11 μm. Further increase in film thickness has negligible impact on its behavior.

**Table 3.3** Photovoltaic parameters of the DSSCs with 0.75 wt% CB/PAniNT with varying thickness in LE and PGE (*CBP_1 is equivalent to CB/PAniNT (0.75) in* ***Table 3.2***).

| Electrolyte | Counter electrode | $V_{OC}$/ V | $J_{SC}$/ mA cm$^{-2}$ | *FF* | *η*/ % |
|---|---|---|---|---|---|
| *Liquid electrolyte* | CBP_1 | 0.75 | 11.86 | 0.67 | 5.96 |
| | CBP_2 | 0.75 | 12.07 | 0.67 | 6.06 |
| | CBP_3 | 0.74 | 12.34 | 0.67 | 6.12 |
| | CBP_4 | 0.74 | 12.52 | 0.71 | 6.62 |
| *Polymer gel electrolyte* | CBP_1 | 0.75 | 8.70 | 0.67 | 4.39 |
| | CBP_2 | 0.78 | 8.86 | 0.67 | 4.41 |
| | CBP_3 | 0.77 | 8.97 | 0.71 | 4.73 |
| | CBP_4 | 0.75 | 9.11 | 0.71 | 4.82 |

**3.3.7 Impedance spectra of the DSSCs.**EIS was used to elucidate the electron transport behavior in DSSCs [47]. Under irradiation, the Nyquist plot (*Z'vs. –Z"*), obtained using the equivalent circuit diagram **(Figure 3.8)**, displays a semicircle in the higher frequency region

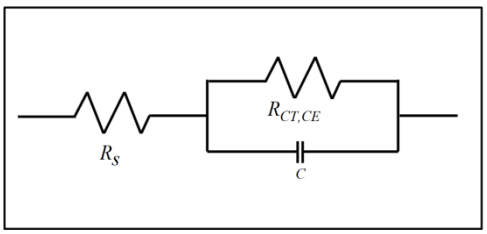


**Figure 3.8** Equivalent circuit diagram for plotting Nyquist plot.

corresponding to charge transfer resistance ($R_{CT,CE}$) at the interface of the CE and electrolyte. $R_{CT,CE}$ is a critical parameter that determines the catalytic activity of the CE towards $I_3^-$ to $I^-$ reduction. Another important parameter is the internal series resistance ($R_S$) of the DSSCs which is an amalgam of the electrolyte resistance and the sheet resistance of the electrode. $R_S$ can be determined from the intercept point on the real axis of Nyquist plot at high frequency. Low values of $R_S$ and $R_{CT,CE}$are indicative of better performance of the DSSCs. 0.75 V was set as the bias potential since the $V_{OC}$ of the DSSCs was obtained near this point. The values for DSSCs with LE having different compositions of CB/PAniNT (0.0, 0.5, 0.75 and 1.0 wt% CB) as CE are given in **Table 3.4(Figure 3.9 (a))**. Initially with pristine PAniNT, the $R_{CT,CE}$value obtained is 1.20 Ω which decreases with addition of CB. An optimized device with 0.75 wt% CB/PAniNT exhibits $R_{CT,CE}$value of 1.06 Ω. The lowering of $R_{CT,CE}$can be attributed to availability of a larger active surface area conferred by both PAniNT and mesoporous CB. Synergistic effect of the combining mode of both the components also provides high conductivity and fast electron transfer passage from CE to the electrolyte. Increased conductivity is considered responsible for

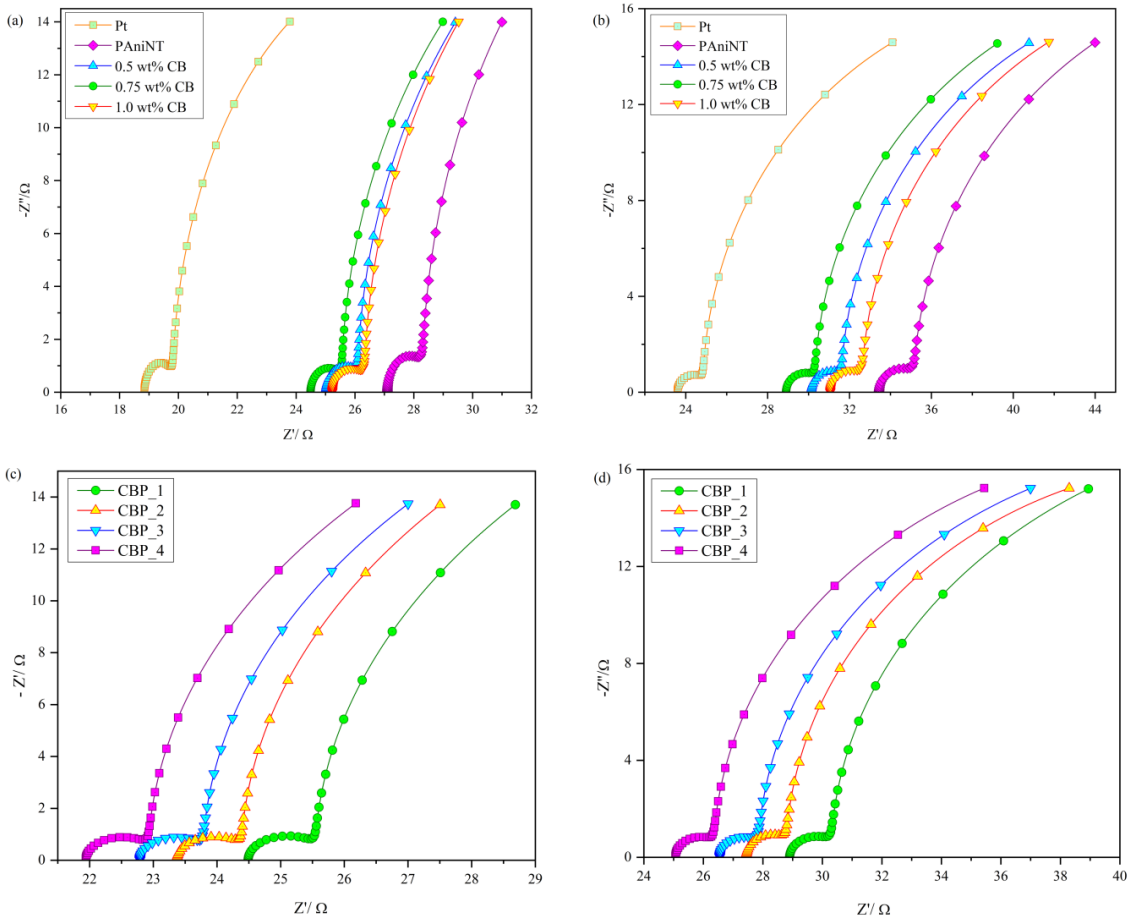


**Figure 3.9** Impedance spectra of DSSCs fabricated with Pt, PAniNT and CB/PAniNT (0.5, 0.75 and 1.0 wt% CB) CE in **(a)** LE and **(b)** PGE, and effect of thickness variation on the impedance spectra of CB/PAniNT (0.75 wt%) based DSSC in **(c)** LE and **(d)** PGE.

lowering the $R_S$ values [11]. Moreover, the electrolyte can be trapped in the pores of CB, enhancing its stability and improving the overall performance of the DSSCs [8]. However, further increment of CB leads to its agglomeration, which lowers the effective surface area of the catalyst. An increase in $R_{CT,CE}$is seen which accelerates electronic recombination and decelerates electrode reaction [8]. Both these effects cause the performance of the DSSCs to deteriorate. A similar trend is observed with PGE where an optimized device with 0.75 wt% CB/PAniNT displays $R_{CT,CE}$value of 1.41 Ω **(Figure 3.9 (b))**. On comparing both the electrolytes, it is seen that the $R_{CT,CE}$values for PGE are higher than those of LE. The magnitude of $R_{CT,CE}$depends on the charge transfer process at electrolyte/CE interface. Thus, higher the number of triiodide ions, better the charge transfer process. But this process is hampered by the polymer network in PGE causing an increase in the $R_{CT,CE}$value.

**Table 3.4** EIS parameters of the DSSCs fabricated with Pt, PAniNT and CB/PAniNT (varying CB content and varying thickness) CE in both LE and PGE.

| Counter electrode | Liquid electrolyte | | Polymer gel electrolyte | |
|---|---|---|---|---|
| | $R_S$/Ω | $R_{CT,CE}$/Ω | $R_S$/Ω | $R_{CT,CE}$/Ω |
| Pt | 18.84 | 0.97 | 23.59 | 1.26 |
| PAniNT | 27.10 | 1.20 | 33.44 | 1.73 |
| CB/PAniNT (0.5) | 25.01 | 1.09 | 30.13 | 1.49 |
| CB/PAniNT (0.75) (equivalent to CBP_1) | 24.49 | 1.06 | 28.90 | 1.41 |
| CB/PAniNT (1.0) | 25.23 | 1.10 | 31.06 | 1.58 |
| CBP_2 | 23.37 | 1.02 | 27.44 | 1.36 |
| CBP_3 | 22.79 | 1.00 | 26.55 | 1.32 |
| CBP_4 | 21.94 | 0.99 | 25.06 | 1.30 |

***Effect of thickness variation:*** The effect of thickness variation on $R_{CT,CE}$and $R_S$ was also studied with EIS by fabricating a series of DSSCs with different thicknesses. In both the types of DSSCs comprising of 0.75 wt% CB/PAniNT as CE, similar trends of decreasing $R_{CT,CE}$and$R_S$with increasing thickness is seen **(Figure 3.9 (c)** and **(d))**. A 0.78 µm thick layer of CE shows $R_{CT,CE}$and$R_S$values of 1.06 Ω and 24.49 Ω for LE, and 1.41 Ω and 28.90 Ω for PGE respectively. Increase in thickness of the CE decreases these values and an optimized device is fabricated with 10.58 µm thick CE. The EIS parameters are tabulated in **Table 3.4**. The main factor contributing

to this result is the electron transfer process. Initially, this process is slightly impaired and the electronic transport resistance is high but increasing thickness results in an augmented active interface which diminishes this effect and leads to better electrocatalytic activity [16].

## 3.4 Conclusion

We have successfully synthesized a novel CB/PAniNT nanocomposite by *in-situ* chemical oxidation polymerization technique. Morphological analysis of the nanocomposite reveals that a layer of mesoporous CB is formed on the surface of PAniNT, causing an increase in the surface area. The resulting nanocomposite has been studied as a potential CE material in DSSCs. CV measurements, EIS analysis and *J-V* characteristic plots show that 0.75 wt% CB/PAniNT exhibits superior electrocatalytic activity towards $I_3^-$ to $I^-$ reduction in contrast to pristine PAniNT. This effect is mainly attributed to an augmented catalytic surface area rendered by incorporation of mesoporous CB. With LE, $\eta$ value of 6.62% has been realized for the nanocomposite with 10.58 μm thick film, while for the same thickness 4.82% efficiency is obtained when PMMA based PGE is used. These values are greatly enhanced in contrast to pristine PAniNT because of a significant decrease in $R_{CT,CE}$with the inclusion of CB. CB/PAniNT nanocomposites, thus, provide an affordable and feasible alternate as a CE material in DSSCs employing both LE and PGE to replace the expensive Pt electrode.

## 3.5 References

[1] O'Regan, B. and Grätzel, M. A low-cost, high-efficiency solar cell based on dye-sensitized colloidal $TiO_2$ films. *Nature*, 353(6346):737-740, 1991.

[2] Choi, H., Kim, H., Hwang, S., Han, Y., and Jeon, M. Graphene counter electrodes for dye-sensitized solar cells prepared by electrophoretic deposition. *Journal of Materials Chemistry*, 21(21):7548-7551, 2011.

[3] Mathew, S., Yella, A., Gao, P., Humphry-Baker, R., Curchod, B. F. E., Ashari-Astani, N., Tavernelli, I., Rothlisberger, U., Nazeeruddin, M. K., and Grätzel, M. Dye-sensitized solar cells with 13% efficiency achieved through the molecular engineering of porphyrin sensitizers. *Nature Chemistry*, 6(3):242-247, 2014.

[4] Nath, B. C., Das, D., Basumatary, J., Ahmed, G. A., and Dolui, S. K. Highly efficient platinum free multi-walled carbon nanotubes/silver nanocomposites as counter electrode for dye sensitized solar cell. *ChemistrySelect*, 1(9):1863-1869, 2016.

[5] Nath, B. C., Mohan, K., Saikia, B. J., Ahmed, G. A., and Dolui, S. K. Designing of platinum free NiS anchored graphene/polyaniline nanocomposites based counter electrode for dye sensitized solar cell. *Journal of Materials Science: Materials in Electronics*, 28(1):1042-1050, 2017.

[6] Miao, X., Pan, K., Pan, Q., Zhou, W., Wang, L., Liao, Y., Tian, G., and Wang, G. Highly crystalline graphene/carbon black composite counter electrodes with controllable content: Synthesis, characterization and application in dye-sensitized solar cells. *Electrochimica Acta*, 96:155-163, 2013.

[7] Li, Q., Wu, J., Tang, Q., Lan, Z., Li, P., Lin, J., and Fan, L. Application of microporous polyaniline counter electrode for dye-sensitized solar cells. *Electrochemistry Communications*, 10(9):1299-1302, 2008.

[8] Zhang, J., Hreid, T., Li, X., Guo, W., Wang, L., Shi, X., Su, H., and Yuan, Z. Nanostructured polyaniline counter electrode for dye-sensitised solar cells: Fabrication and investigation of its electrochemical formation mechanism. *Electrochimica Acta*, 55(11):3664-3668, 2010.

[9] Qin, Q. and Zhang, R. A novel conical structure of polyaniline nanotubes synthesized on ITO-PET conducting substrate by electrochemical method. *Electrochimica Acta*, 89:726-731, 2013.

[10] Park, K.-H., Kim, S. J., Gomes, R., and Bhaumik, A. High performance dye-sensitized solar cell by using porous polyaniline nanotubes as counter electrode. *Chemical Engineering Journal*, 260:393-398, 2015.

[11] Chen, J., Li, B., Zheng, J., Zhao, J., Jing, H., and Zhu, Z. Polyaniline nanofiber/carbon film

as flexible counter electrodes in platinum-free dye-sensitized solar cells. *Electrochimica Acta*, 56(12):4624-4630, 2011.

[12] Wu, M., Lin, X., Wang, T., Qiu, J., and Ma, T. Low-cost dye-sensitized solar cell based on nine kinds of carbon counter electrodes. *Energy and Environmental Science*, 4(6):2308-2315, 2011.

[13] Murata, K., Imoto, K., Komura, T., Yamaguchi, T., Takahashi, K., and Nakamura, J. High-performance carbon counter electrode for dye-sensitized solar cells. *Solar Energy Materials and Solar Cells*, 79(4):459-469, 2003.

[14] Huang, Z., Liu, X., Li, K., Li, D., Luo, Y., Li, H., Song, W., Chen, L., and Meng, Q. Application of carbon materials as counter electrodes of dye-sensitized solar cells. *Electrochemistry Communications*, 9(4):596-598, 2007.

[15] Murakami, T. N. and Grätzel, M. Counter electrodes for DSC: Application of functional materials as catalysts. *Inorganica Chimica Acta*, 361(3):572-580, 2008.

[16] Murakami, T. N., Ito, S., Wang, Q., Nazeeruddin, M. K., Bessho, T., Cesar, I., Liska, P., Humphry-Baker, R., Comte, P., Péchy, P., and Grätzel, M. Highly efficient dye-sensitized solar cells based on carbon black counter electrodes. *Journal of The Electrochemical Society*, 153(12):A2255, 2006.

[17] Cochet, M., Maser, W. K., Benito, A. M., Callejas, M. A., Martínez, M. T., Benoit, J. M., Schreiber, J., and Chauvet, O. Synthesis of a new polyaniline/nanotube composite: "*In-situ*" polymerisation and charge transfer through site-selective interaction. *Chemical Communications*, 1(16):1450-1451, 2001.

[18] Sun, H., Luo, Y., Zhang, Y., Li, D., Yu, Z., Li, K., and Meng, Q. In situ preparation of a flexible polyaniline/carbon composite counter electrode and its application in dye-sensitized solar cells. *The Journal of Physical Chemistry C*, 114(26):11673-11679, 2010.

[19] Wang, G., Xing, W., and Zhuo, S. The production of polyaniline/graphene hybrids for use as a counter electrode in dye-sensitized solar cells. *Electrochimica Acta*, 66:151-157, 2012.

[20] Ikeda, N., Teshima, K., and Miyasaka, T. Conductive polymer-carbon-imidazolium composite: A simple means for constructing solid-state dye-sensitized solar cells. *Chemical Communications*, 0(16):1733-1735, 2006.

[21] Wu, J., Lan, Z., Lin, J., Huang, M., and Li, P. Effect of solvents in liquid electrolyte on the photovoltaic performance of dye-sensitized solar cells. *Journal of Power Sources*, 173(1):585-591, 2007.

[22] Mohan, K., Bora, A., Nath, B. C., Gogoi, P., Saikia, B. J., and Dolui, S. K. A highly stable and efficient quasi solid state dye sensitized solar cell based on polymethyl methacrylate (PMMA)/polyaniline nanotube (PANI-NT) gel electrolyte. *Electrochimica Acta*, 222:1072-1078, 2016.

[23] Xue, P., Bao, Y., Li, Q., and Wu, C. Impact of modification of carbon black on morphology and performance of polyimide/carbon black hybrid composites. *Physical Chemistry Chemical Physics*, 12(37):11342-11350, 2010.

[24] Rositani, F., Antonucci, P. L., Minutoli, M., Giordano, N., and Villari, A. Infrared analysis of carbon blacks. *Carbon*, 25(3):325-332, 1987.

[25] Wang, H., Hao, Q., Yang, X., Lu, L., and Wang, X. A nanostructured graphene/polyaniline hybrid material for supercapacitors. *Nanoscale*, 2(10):2164-2170, 2010.

[26] Jawhari, T., Roid, A., and Casado, J. Raman spectroscopic characterization of some commercially available carbon black materials. *Carbon*, 33(11):1561-1565, 1995.

[27] Ye, M., Wen, X., Wang, M., Iocozzia, J., Zhang, N., Lin, C., and Lin, Z. Recent advances in dye-sensitized solar cells: From photoanodes, sensitizers and electrolytes to counter electrodes. *Materials Today*, 18(3):155-162, 2015.

[28] Kuchibhatla, S. V. N. T., Karakoti, A. S., Bera, D., and Seal, S. One dimensional nanostructured materials. *Progress in Materials Science*, 52(5):699-913, 2007.

[29] Dauginet-De Pra, L. and Demoustier-Champagne, S. Investigation of the electronic structure and spectroelectrochemical properties of conductive polymer nanotube arrays. *Polymer*, 46(5):1583-1594, 2005.

[30] Li, Y., Bober, P., Apaydin, D. H., Syrový, T., Sariciftci, N. S., Hromádková, J., Sapurina, I., Trchová, M., and Stejskal, J. Colloids of polypyrrole nanotubes/nanorods: A promising conducting ink. *Synthetic Metals*, 221(221):67-74, 2016.

[31] Parthasarathy, R. V. and Martin, C. R. Template-synthesized polyaniline microtubules. *Chemistry of Materials*, 6(10):1627-1632, 1994.

[32] Konyushenko, E. N., Stejskal, J., Šeděnková, I., Trchová, M., Sapurina, I., Cieslar, M., and Prokeš, J. Polyaniline nanotubes: Conditions of formation. *Polymer International*, 55(1):31-39, 2006.

[33] Reddy, K. R., Sin, B. C., Ryu, K. S., Noh, J., and Lee, Y. *In situ* self-organization of carbon black-polyaniline composites from nanospheres to nanorods: Synthesis, morphology, structure and electrical conductivity. *Synthetic Metals*, 159(19):1934-1939, 2009.

[34] Gong, F., Xu, X., Zhou, G., and Wang, Z. S. Enhanced charge transportation in a polypyrrole counter electrode via incorporation of reduced graphene oxide sheets for dye-sensitized solar cells. *Physical Chemistry Chemical Physics*, 15(2):546-552, 2013.

[35] Sun, W., Peng, T., Liu, Y., Xu, S., Yuan, J., Guo, S., and Zhao, X.-Z. Hierarchically porous hybrids of polyaniline nanoparticles anchored on reduced graphene oxide sheets as counter electrodes for dye-sensitized solar cells. *Journal of Materials Chemistry A*, 1(8):2762-2768, 2013.

[36] Li, P., Wu, J., Lin, J., Huang, M., Huang, Y., and Li, Q. High-performance and low platinum loading Pt/carbon black counter electrode for dye-sensitized solar cells. *Solar Energy*, 83(6):845-849, 2009.

[37] Nelson, I. V. and Iwamoto, R. T. Voltammetric evaluation of the stability of trichloride, tribromide, and triiodide ions in nitromethane, acetone, and acetonitrile. *Journal of Electroanalytical Chemistry (1959)*, 7(3):218-221, 2002.

[38] Mathew, A., Anand, V., Rao, G. M., and Munichandraiah, N. Effect of iodine concentration on the photovoltaic properties of dye sensitized solar cells for various $I_2$/LiI ratios. *Electrochimica Acta*, 87:92-96, 2013.

[39] Kopidakis, N., Benkstein, K. D., van de Lagemaat, J., and Frank, A. J. Transport-limited recombination of photocarriers in dye-sensitized nanocrystalline $TiO_2$ solar cells. *The Journal of Physical Chemistry B*, 107(41):11307-11315, 2003.

[40] Lyon, L. A. and Hupp, J. T. Energetics of semiconductor electrode/solution interfaces: EQCM evidence for charge-compensating cation adsorption and intercalation during accumulation layer formation in the titanium dioxide/acetonitrile system. *The Journal of Physical Chemistry*, 99(43):15718-15720, 1995.

[41] Zeng, X.-R. and Ko, T.-M. Structure-conductivity relationships of iodine-doped polyaniline. *Journal of Polymer Science, Part B: Polymer Physics*, 35(13):1993-2001, 1997.

[42] Hao, F., Lin, H., Zhang, J., Zhuang, D., Liu, Y., and Li, J. Influence of iodine concentration on the photoelectrochemical performance of dye-sensitized solar cells containing non-volatile electrolyte. *Electrochimica Acta*, 55(24):7225-7229, 2010.

[43] Nei De Freitas, J., Nogueira, A. F., and De Paoli, M. A. New insights into dye-sensitized solar cells with polymer electrolytes. *Journal of Materials Chemistry*, 19(30):5279-5294, 2009.

[44] Yu, Z., Gorlov, M., Nissfolk, J., Boschloo, G., and Kloo, L. Investigation of iodine concentration effects in electrolytes for dye-sensitized solar cells. *The Journal of Physical Chemistry C*, 114(23):10612-10620, 2010.

[45] Ameen, S., Shaheer Akhtar, M., Kim, Y. S., Yang, O. B., and Shin, H. S. Sulfamic acid-doped polyaniline nanofibers thin film-based counter electrode: Application in dye-sensitized solar cells. *The Journal of Physical Chemistry C*, 114(10):4760-4764, 2010.

[46] Papageorgiou, N. Counter-electrode function in nanocrystalline photoelectrochemical cell configurations. *Coordination Chemistry Reviews*, 248(13-14):1421-1446, 2004.

[47] Adachi, M., Sakamoto, M., Jiu, J., Ogata, Y., and Isoda, S. Determination of parameters of electron transport in dye-sensitized solar cells using electrochemical impedance spectroscopy. *The Journal of Physical Chemistry B*, 110(28):13872-13880, 2006.